ACS SENSORS

pubs.acs.org/acssensors Article

Sensitive Bioassay with an Ultralarge Dynamic Range via Microlaser Ensemble Quenching

Weishu Wu, Yuhang Cao, Xiaotian Tan, and Xudong Fan*

Cite This: ACS Sens. 2025, 10, 6436−6445 Read Online

ACCESS | Metrics & More | Article Recommendations | Supporting Information

ABSTRACT: We present a bioassay platform that leverages the lasing threshold distribution in a microlaser ensemble (ME), consisting of hundreds of individual microlasers, to measure analyte concentrations in solution. An ME is formed by placing dye-doped microbeads in a micro Fabry−Perot cavity. The microbeads are surface-modified with biorecognition molecules to capture analytes, while the quenchers resulting from the presence of the analytes on the microbeads' surfaces increase the lasing thresholds of the microlasers. Since the number of analytes varies from one microbead (or microlaser) to another due to the randomness in binding processes, a distribution of the analytes (and hence the quenchers) in the ME is created, which in turn leads to a lasing threshold distribution in the ME. Experimentally, multiple pumping energy densities are used to probe the lasing threshold distribution. A theoretical model is used to map the lasing threshold distribution to the analyte distribution in the ME, and then to recover the analyte concentration in solution. Using streptavidin as a model system, our platform achieves a detection limit of 0.1 pg/mL and a dynamic range exceeding 5 orders of magnitude, showing that the ME quenching method can provide a low detection limit with a superior dynamic range.

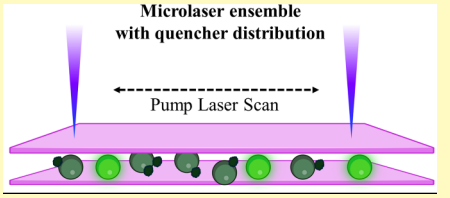

KEYWORDS: *microlaser, microlaser ensemble, microlaser quenching, digital bioassay, ELISA*

The goal of a bioassay is to quantify target analytes (such as biomolecules) in a sample. Their core working principle is to convert the presence of the target analytes into measurable signals. Among the various methods, enzyme-linked immunosorbent assay (ELISA) is a commonly used technique,[1,2] in which detection antibodies conjugated with enzymes bind to the captured target analytes and the enzyme−substrate reaction causes the substrate to emit light (such as chemiluminescence)[3,4] or change its color (colorimetric detection).[5,6] Alternatively, detection antibodies can be conjugated with fluorescent labels[7] such as dyes,[8] quantum dots,[9−11] and plasmonic nanoparticles (i.e., metal nanoparticles).[12−14] The light signal from these labels is measured to quantify the target analyte concentration. Since the measured signal varies continuously with the concentration of the analyte, these traditional approaches are referred to as analog detection. Such methods are highly refined, widely available in commercial kits, and typically achieve detection ranges from a few picograms per milliliter (pg/mL) to tens of thousands of pg/mL, depending on the specific assay formats, reagents, and target analytes.[15−19]

To further improve the detection limit of bioassays, digital ELISA was developed.[20−27] This approach enables detecting extremely low analyte concentrations by allocating individual analyte molecules to an ensemble of microunits (such as microbeads) and then counting the fraction of these microunits that emit light (bright microunits). Under the assumption that each microunit has no more than one analyte molecule associated with it, detection of the analyte concentration becomes analyzing the distribution of the bright microunits and calculating its mean value according to the Poisson distribution. Commercial examples, such as Quanterix's bead-based digital ELISA, can detect cytokines as low as 0.01 pg/mL.[20,28−30] Other works have employed alternative labeling methods, such as plasmonic nanoparticles,[31,32] fluorescent dyes,[33,34] and quantum dots,[35,36] to replace the enzyme labels.[23,25−27] However, these digital immunoassays have a limited dynamic range. For example, the upper detection limit of Quanterix's bead-based method is only 24 pg/mL.[29,30] At higher concentrations, the assumption for digital ELISA, that is, the average number of analytes per microbead should be far below 1, breaks down.[37] In order to extend the dynamic range of digital ELISA, samples under test need to be serially diluted so that the concentration of the target analytes falls in the range allowed by digital ELISA. However, the appropriate dilution factor needs to be determined through multiple trials. Other strategies have also been explored, including stitching the digital detection calibration curve with the analog detection calibration curve[21,27] or extrapolating the calibration curve beyond the

Received: January 21, 2025
Revised: August 26, 2025
Accepted: August 28, 2025
Published: September 4, 2025

https://doi.org/10.1021/acssensors.5c00251
ACS Sens. 2025, 10, 6436−6445

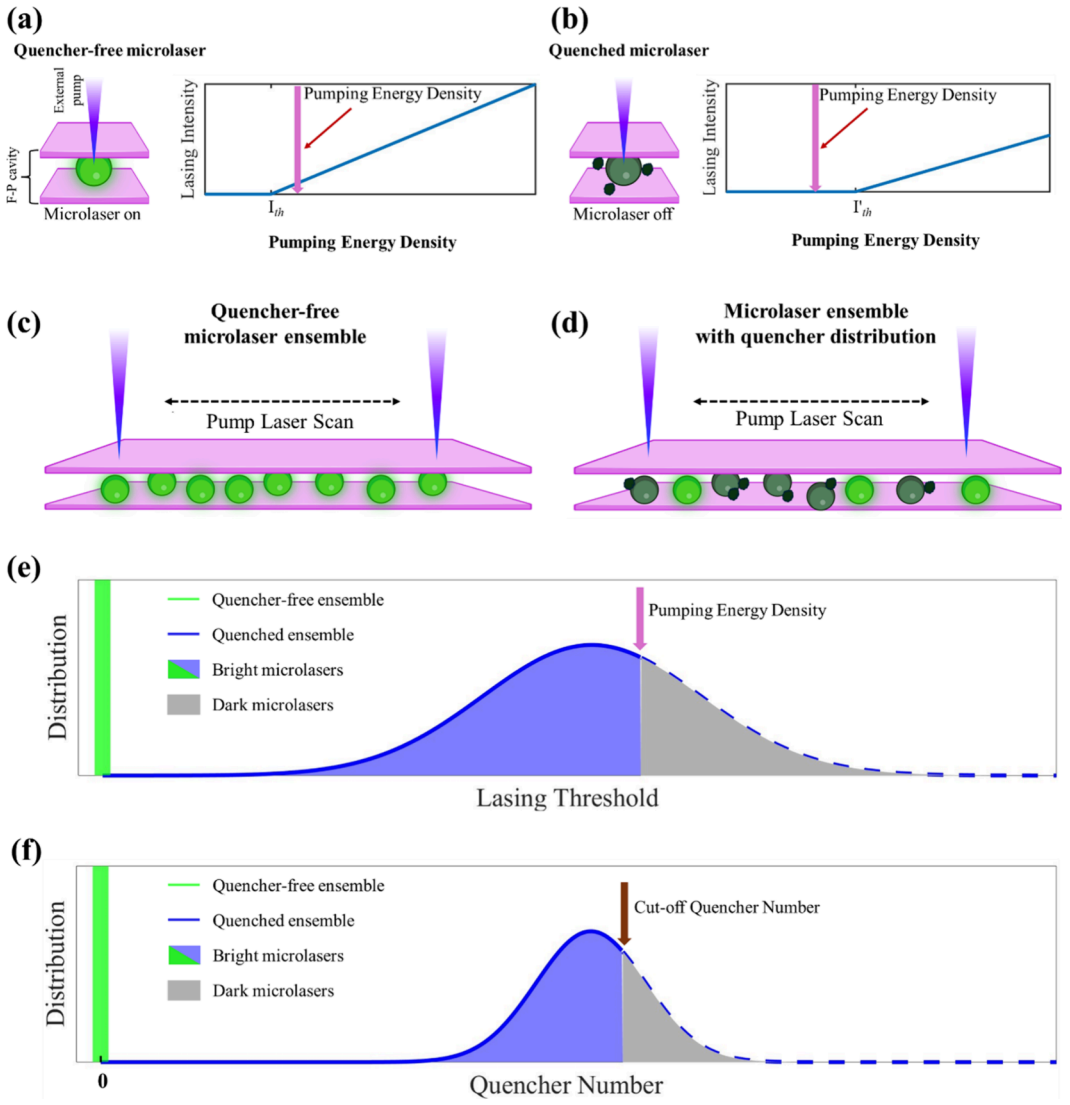

Figure 1. Conceptual illustration of the microlaser ensemble (ME) quenching bioassay. (a) A single microlaser is formed by placing a microbead doped with laser gain medium (such as dye) into a liquid-filled micro Fabry−Perot (F−P) cavity (liquid medium not shown for clarity). The microlaser emits laser signals (bright microlaser) when the external pumping exceeds its lasing threshold. (b) If the microbead has quenchers near or on its surface due to the analytes captured by the microbead, its lasing threshold can surpass the pumping energy density, thus turning off the laser emission (dark microlaser). (c) A microlaser ensemble refers to a group of identical dye-doped microbeads deposited in the same F−P cavity. When the external pumping exceeds the lasing threshold, all the microlasers in the ME emit laser signals (bright microlasers). (d) When the ME is exposed to the sample under test, due to the randomness of the analyte binding to the microlasers, different microlasers have different numbers of analytes (and hence quenchers) associated with them. Consequently, the lasing threshold of each microlaser increases according to the number of quenchers near or on its surface, thus creating a lasing threshold distribution within the ME. Under the same external pump, some microlasers are quenched (dark microlasers), whereas the rest of microlasers still have laser emission (bright microlasers). (e) Illustration of measuring the lasing threshold distribution in an ME. Quencher-free microlasers have the same lasing threshold as shown by the d-function-like green line on the left. The quencher distribution in the microlaser ensemble leads to a distribution of the lasing threshold as represented by the blue curve. Under a given pumping energy density, the microlasers in the blue-shaded area, which have the lasing threshold lower than the pumping energy density, are bright microlasers, whereas the microlasers in the gray-shaded area are quenched microlasers (dark microlasers). By counting the bright microlasers within the ensemble when the pumping energy density is varied, the lasing threshold distribution can be mapped. (f) Mapping the lasing threshold distribution is equivalent to mapping the quencher distribution and hence the analyte distribution within the microlaser ensemble, which is in turn related to the analyte concentration in solution. The d-function-like green line on the left represents the situation where none of the microlasers in the ensemble has a quencher on or near the microbead surface.

single molecule assumption.[38] However, these attempts face issues. It is difficult to determine the cutoff (or transition) analyte concentration between the digital detection mode and analog detection mode[21,27] and there may be discontinuity in digital and analog calibration curves due to two completely different methods used to obtain digital and analog sensing signals.[38] Furthermore, extrapolating the calibration curve leads to large errors. Therefore, a unified method that has a high dynamic range to cover both the lower and the upper end of the analyte concentration without any artificially introduced digital-to-analog transition is highly desirable.

In this work, we propose a microlaser ensemble (ME) quenching bioassay platform that achieves both a low detection limit and a large dynamic range. In this method, individual

https://doi.org/10.1021/acssensors.5c00251
ACS Sens. 2025, 10, 6436−6445

microlasers are used as detection microunits. First, these microlasers are exposed to the analytes in solution and subsequently capture the analytes through biochemical interactions (such as antibody−antigen binding). The presence of the analytes in these microlasers alters their lasing thresholds through the quenchers produced by enzyme−substrate reactions. When the external pumping varies, the laser emission from some of the microlasers in the ME persists, whereas other microlasers are completely quenched, depending on the number of quenchers (and hence the analytes) associated with each microlaser. As a result, the distribution of the analytes on the ME can be established, which allows us to recover the analyte concentration in solution through a statistical model. This platform achieves a detection limit of 0.1 pg/mL and a dynamic range spanning more than 5 orders of magnitude without any calibration curve stitching/extrapolation or sample dilution. We foresee that this highly sensitive platform with a large dynamic range and the related statistical method will find broad real-world applications.

WORKING PRINCIPLE

Without losing generality, in this work, we use a microlaser formed by placing a dye-doped microbead along with a liquid medium into a micro Fabry−Perot (F−P) cavity (Figure 1a). Each microbead, together with the F−P cavity, is treated as an individual detection microunit. Other forms of the microunits, such as ring resonator lasers,[39,40] nanowire lasers,[41] and vertical-cavity surface-emitting lasers (VCSELs), can also be used.

A single microlaser formed by a dye-doped microbead in an F−P cavity has been extensively studied previously by our group.[42] When a microlaser is pumped by an external laser at an energy density higher than its lasing threshold, it emits laser signals. We refer to it as a bright microlaser, as illustrated in Figure 1a. For the same microlaser, when it captures analytes, which results in light absorbing molecules (quenchers) to be near or on the microbead surface (through a process such as enzyme−substrate reaction), the lasing threshold increases. When the lasing threshold surpasses the external pumping energy density, the microlaser is quenched (a dark microlaser), as illustrated in Figure 1b.

We now move from a single microlaser to an ME, which is composed of many identical microlasers. In a quencher-free state, when an ME is pumped at an energy density slightly higher than a microlaser's lasing threshold, all microlasers are bright (Figure 1c). When the ME goes through analyte-capturing and quencher-generating processes, the randomness of the analyte binding to the microbeads leads to a distribution of the analytes on the microlasers, which in turn causes a distribution of quenchers and hence lasing thresholds within the ME. Under a given external pumping energy density, only a portion of the microlasers, whose lasing thresholds are lower than the pumping energy density, remain bright, as shown in Figure 1d.

Figure 1e presents the distribution of the lasing threshold. For the case of Figure 1c (quencher-free), the lasing threshold for all microlasers is the same and low, as represented by the δ-function like green line on the left. Correspondingly, the number of quenchers on the microlaser is zero and its distribution is a δ function (the green line in Figure 1f). For the case of Figure 1d, the initial δ-function like threshold distribution in Figure 1e starts to shift to larger values and spread. The microlasers whose lasing thresholds are on the left side of the distribution curve (i.e., the lasing thresholds are lower than the pumping energy density) remain bright, whereas those on the right side (i.e., the lasing thresholds are higher than the pumping energy density) become dark (or quenched). By changing the external pumping energy density and counting the fraction of the bright microlasers (which is the cumulative distribution of the lasing threshold), we can map the distribution of the lasing threshold and hence the underlying distribution of quenchers on the microlasers shown in Figure 1f. With the known quencher distribution, we can recover the analyte distribution on the microlasers and hence the analyte concentration in solution through a statistical model.

THEORETICAL MODEL

We developed the microlaser quenching equation (MQE) for the ME to study the relationship between the lasing thresholds of microlasers and the number of analytes they capture. The MQE, as shown in eq 1, is built on well-recognized theoretical models for microlasers[43−46] and an assumption that the quencher production rate is proportional to the number of enzymes, which is in turn proportional to the number of analytes captured by the microlasers. The equation:

$$k_j = \frac{\ln\left(\frac{I_{\mathrm{th}(j)}^{\mathrm{exp}} + I_{\mathrm{norm}}}{I_0 + I_{\mathrm{norm}}}\right)}{E} \tag{1}$$

states that for the j_{th} microlaser in the ensemble with the quencher-free lasing threshold, I_0, its experimentally measured lasing threshold, $I_{\mathrm{th}(j)}^{\mathrm{exp}}$, can be used to recover the number of analytes k_j associated with the microlaser. E, I_0, and I_{norm} are the three fitting parameters determined by the experimental setup. The detailed derivation of eq 1 can be found in our theoretical analysis.[47]

When the ME is exposed to the analytes in solution, the analyte molecules bind to the microlasers through interactions such as antigen−antibody binding. The binding processes are affected by the random movement of the analyte molecules, leading to a distribution of the analytes on the microlasers, which can be experimentally measured in the following way.

When the ME is pumped at multiple pumping energy densities, a data pair $[(Lf(i), I_{\mathrm{pump}}^{\mathrm{exp}}(i))]$ can be obtained, where $Lf(i)$ is the lasing fraction of the ME at the pumping energy density of $I_{\mathrm{pump}}^{\mathrm{exp}}(i)$. As discussed in the Working Principle section, the lasing fraction is equivalent to the fraction of microlasers with the number of analytes smaller than a specific value.

In our experiments, the number of microlasers is always lower than the number of analytes in the test sample, that is, the average number of analytes per microlaser is larger than one. From the central limit theorem, we infer that the distribution of the analytes on the microlasers follows a Gaussian distribution. Therefore, from eq 1, the lasing fraction of the ME, $Lf(i)$, and its paired measured pumping energy density, $I_{\mathrm{pump}}^{\mathrm{exp}}(i)$, should follow a Gaussian cumulative distribution:

$$Lf(i) = \phi_{cumu}\left(\frac{\ln\left(\frac{I_{pump}^{\mathrm{exp}}(i) + I_{norm}}{I_0 + I_{norm}}\right)}{E}; \mu, \sigma\right) \tag{2}$$

https://doi.org/10.1021/acssensors.5c00251
ACS Sens. 2025, 10, 6436−6445

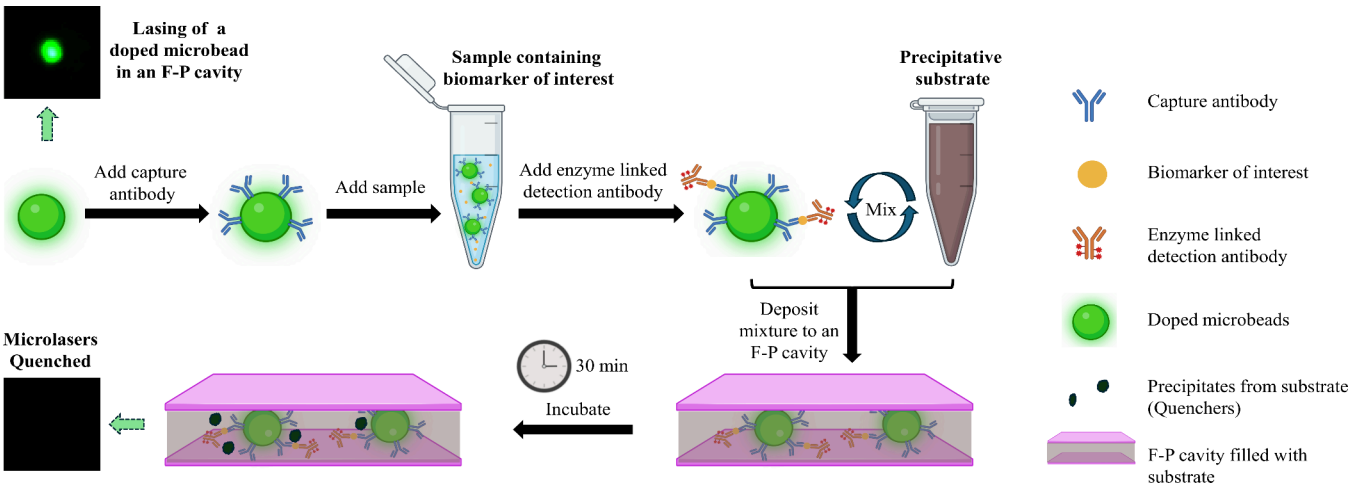

Figure 2. Illustration of the microlaser ensemble quenching bioassay. For clarity, only one or two microlasers are used to represent the process for the whole ensemble. First, dye-doped microbeads, conjugated with capture antibodies, are incubated with the sample under test. After the biomarkers are captured, enzyme-linked detection antibodies are added and bound to the microbeads, which are subsequently mixed with substrate solution. The mixture is deposited into an F−P cavity, where enzyme−substrate reaction produces precipitations that work as quenchers for the microlasers, producing a distribution of the lasing threshold. This lasing threshold distribution can be measured by changing the external pumping energy density and subsequently used to calculate the analyte concentration. The image on the top left corner shows laser emission from a microlaser (i.e., dye-doped microbead in an F−P cavity). The image on the bottom left corner shows the laser emission from the microlaser is quenched.

,where ϕ_{cumu} is the cumulative Gaussian distribution function. μ and σ are the mean and standard deviation for this Gaussian distribution, respectively, which can be obtained via function fitting. μ is related to the analyte concentration in solution. Such a relationship can be established by calibration curves obtained experimentally, which will be discussed later in the Results section.

To quantitatively recover the analyte concentration, we introduce a new parameter, the recovered mean lasing threshold, I_μ, which is connected to μ via the following equation.

$$\mu = \frac{\ln\left(\frac{I_\mu + I_{norm}}{I_0 + I_{norm}}\right)}{E} \tag{3}$$

or

$$I_\mu = (I_0 + I_{norm})e^{\mu E} - I_{norm} \tag{4}$$

Note that the invariable product of μE is used in eq 4 and therefore the I_μ value is unique. I_μ can be deemed as the lasing threshold that corresponds to an imaginary microlaser with the averaged number (μ) of quenchers. Using the calibration relation between the experimentally fitted I_μ and the analyte concentration, we can use eq 4 to recover the analyte concentration. I_0 and I_{norm} are fitting parameters obtained from data fitting using the experiment data. I_0 is the mean lasing threshold for the ME that was incubated with the negative control group (both the analyte concentration and k are 0). The detection limit can therefore be defined as the concentration whose corresponding I_μ is at least σ_{exp} higher than I_0. σ_{exp} is the standard deviation for I_μ from experimental data.

MATERIALS AND METHODS

ME Quenching Bioassay Protocol. We present a bioassay protocol for the ME quenching experiments in Figure 2. As shown in the top panel of Figure 2, before the microbeads were placed into an F−P cavity to form the ME, they underwent a surface modification step, an analyte capture step, and a labeling step. First, dye-doped microbeads (mean diameter: 5 μm, FCDG008, Bangs Laboratories Inc., USA) were surface modified and conjugated with the desired capture antibodies using a conjugation kit (PL01N, Bangs Laboratories Inc., USA) and following manufacturer's protocols. The microbeads were then incubated with 200 μL SuperBlock (37515, Thermo Fisher, USA) for 60 min followed by two repeated wash (PBS) steps. The microbeads were gently rotated during each incubation step using a rotator (R2020, Benchmark Scientific, USA). For the analyte capture step, the test sample (200 μL) was mixed with functionalized microbeads and incubated for 60 min followed by two repeated wash (PBS) steps. For the labeling step, the microbeads were incubated with biotinylated detection antibodies (200 μL) for 60 min, followed by two repeated wash (PBS) steps, and then with 200 μL of 1:250 diluted streptavidin poly-HRP (21140, Thermo Fisher, USA) for 30 min followed by three repeated wash steps (PBS). The microbead suspension was centrifuged at 400 g for 15 min to complete liquid exchange. For IL-6 ELISA experiments, antibody sets from a test kit were used (DY206, R&D Systems, USA).

Finally, these microbeads, now with captured analytes and labeled with poly-HRP, were mixed with precipitative substrate solution and immediately loaded into an F−P cavity to form the ME (see the lower panel of Figure 2). The F−P cavity consisted of two highly reflective mirrors (Evaporated Coatings, Inc., USA),[48,49] each of 1″ by 1″. The spacing of the F−P cavity was controlled by the dye-doped microbeads (i.e., 5 μm). We used a 1:1 mixture of 10x concentrated metal-enhanced DAB (34065, Thermo Fisher, USA) and concentrated hydrogen peroxide (34062, Thermo Fisher, USA) as the substrate (50 μL) in this procedure. The mixture was incubated in the F−P cavity for 30 min so that abundant precipitates that act as quenchers for microlasers could form. Although for each analyte concentration, ∼10,000 microbeads were used to incubate with the sample and subsequently loaded into the F−P cavity. In the measurement and data analysis step, we processed only ∼1000 microlasers located at the center of the F−P cavity. Therefore, the number of microlasers in an ME was ∼1000.

We also used a simpler biotin−streptavidin binding assay to evaluate our platform. In this simplified assay, biotinylated antibodies (MQ2-39C3, Thermo Fisher, USA) were conjugated to the surface of the microbeads using the same conjugation kit mentioned previously (PL01N, Bangs Laboratories Inc., USA). Streptavidin conjugated with

https://doi.org/10.1021/acssensors.5c00251
ACS Sens. 2025, 10, 6436−6445

poly-HRP served as the analyte, which was captured by biotin on the microbeads through a 20 min of incubation. The microbeads were then washed three times and mixed with the substrate solution in the same manner as the standard ME quenching immunoassay protocol described above before they were loaded into an F−P cavity.

Lasing Threshold Measurements of the ME. In the measurement step, the ME (i.e., an F−P cavity with microbeads and quenchers in it) was placed under a custom-built laser emission microscope where an external nanosecond laser source (473 nm, 5 kHz repetition rate) was used to scan over the microlasers, and the images were taken. Details of the laser emission microscope can be found in our previous publications.[48,49] A white light image of the microbeads within the F−P cavity was taken to exactly count the total number of microlasers. The ME was pumped at six pumping energy densities (25, 45, 90, 125, 250, and 400 $\mu J/mm^2$) and the corresponding lasing fraction of the ME for each pumping energy density was recorded. The total number of microlasers, and the number of bright microlasers were counted using a fine-tuned YOLO-v8 model. An example of microlaser counting can be found in Section S1 in the Supporting Information.

RESULTS

Demonstration of Microlaser Quenching. We first investigated the quenching of microlasers by enzyme−substrate reactions and optimized the assay protocol to determine the enzyme−substrate incubation time. A biotin−streptavidin binding assay using a fixed 1 ng/mL of streptavidin poly-HRP was performed. The four sets of MEs were prepared in the same manner according to the assay procedures described in the Materials and Methods section, except that incubation time with substrate was chosen to be 0, 10, 20, and 30 min, respectively. Each set of the ME was scanned at six selected pumping energy densities.

Figure 3a shows an exemplary microlaser from each set of the ME with a fixed incubation time, illustrating how the increased incubation time affects the microlasers. As incubation time increases from 0 min (bottom row) to 30 min (top row), the microlasers' lasing thresholds increase progressively, meaning that they may be quenched more easily at a lower pumping energy density. Figure 3b provides more quantitative analysis of the four sets of the MEs. It shows that the MEs with longer incubation times exhibit lower lasing fractions, as more quenchers can form. In subsequent experiments, we chose an incubation time of 30 min to achieve a strong quenching effect. Note that the incubation time here refers to the enzyme−substrate reaction time, which is an additional period on top of sample loading and other procedure-related time during the experiment.

From Figure 3b, we can see that the lasing fraction is lower than 100%, even at a high pumping energy density (400 $\mu J/mm^2$), which suggests that there exist "bad" microlasers whose gain cannot overcome the cavity loss and/or the loss caused by quenchers. While the exact reasons for "bad" microlasers are unknown, we speculate that this could be due to some microbeads having a very low dye doping density or whose shape deviates far from spherical, which causes a higher cavity loss. The effect of these "bad" microlasers (i.e., those that do not lase at the highest pumping energy density, 400 $\mu J/mm^2$ in this work) will be removed from our data analysis in the next section by normalization.

A Biotin−Streptavidin Binding Assay. We tested the ME quenching bioassay using a biotin−streptavidin binding assay. The protocol is a simplified version of immunoassays described in the Materials and Methods section. After conjugation of biotinylated antibodies, the microbeads were

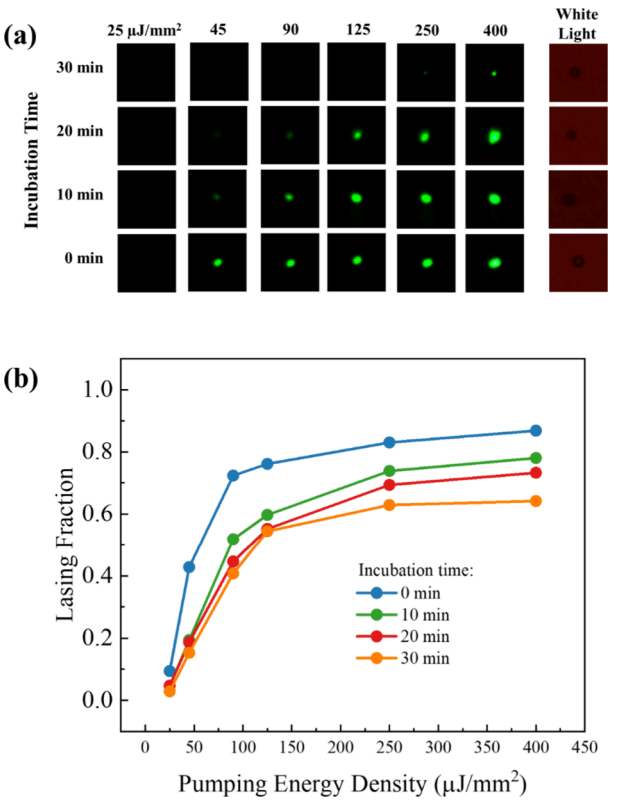

Figure 3. (a) Example of a microlaser at various pumping energy densities over various incubation times. Each image has dimensions of 35 μm × 35 μm. The rightmost column contains white light images of the microlaser (microbead). (b) Change in the lasing fraction within the same microlaser ensemble with respect to incubation time. Quenchers formed within the microlasers over time gradually increase microlasers' lasing thresholds, thus gradually reducing the lasing fraction in the ME under a fixed pumping energy density. Streptavidin poly-HRP = 1 ng/mL.

separated into 13 equal portions, including 12 positive samples, incubated in 12 five-fold, serial-diluted streptavidin poly-HRP solutions and 1 negative control sample (containing 0 pg/mL streptavidin poly-HRP). For each of the 13 portions of microbeads, we created a corresponding set of ME by placing the microbeads in an F−P cavity, as described in the Materials and Methods.

Figure 4a shows the lasing fraction of the 13 sets of MEs under various pumping energy densities. It is seen that for a given set of ME that corresponds to a fixed analyte concentration, the lasing fraction increases with the increased pumping energy density. If we regroup these data points based on each pumping energy density, which are plotted in six colored curves, it is seen that within each curve (i.e., under the same pumping energy density) the lasing fraction decreases with the increased analyte concentration and hence increased number of quenchers associated with the microlasers. As discussed in Figure 3, there exist "bad" microlasers that may not lase even at the highest pumping energy density (400 $\mu J/mm^2$ in our case), which may affect our lasing fraction calculation. To remove the impact of the "bad" microlasers, in Figure 4b we normalize each lasing fraction curve to the corresponding lasing fraction obtained with the negative control, that is, when the analyte (streptavidin) concentration is 0 pg/mL (or 10^{-5} pg/mL in the logarithmic scale). Details of the normalization description can be found in the

https://doi.org/10.1021/acssensors.5c00251
ACS Sens. 2025, 10, 6436−6445

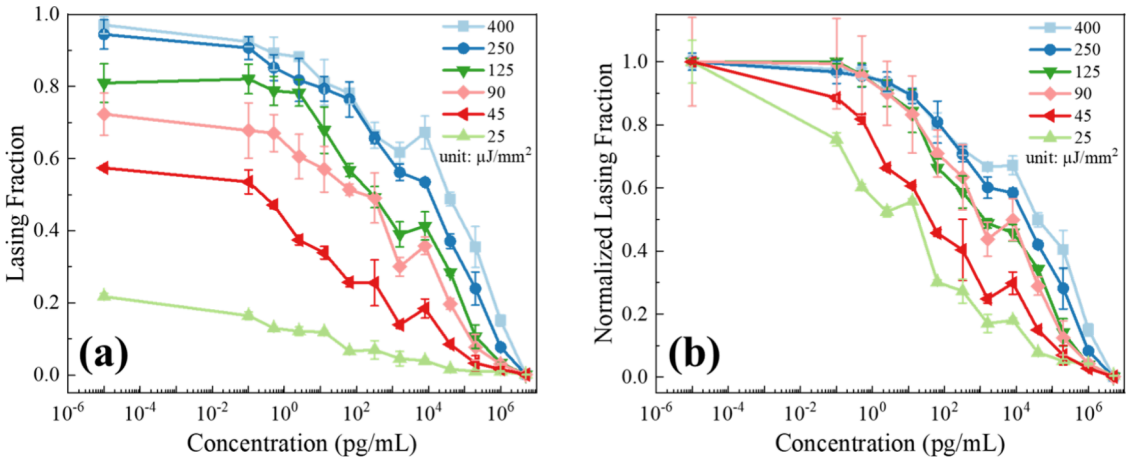

Figure 4. Lasing fraction of the MEs with respect to the analyte (streptavidin) concentration under various pumping energy densities. (a) Raw data. (b) Normalized to the zero analyte concentration for each pumping energy density. Note that in the logarithmic scale in the x-axis, we use 10^{-5} pg/mL to represent the zero analyte concentration. Error bars are obtained with triplicate measurements.

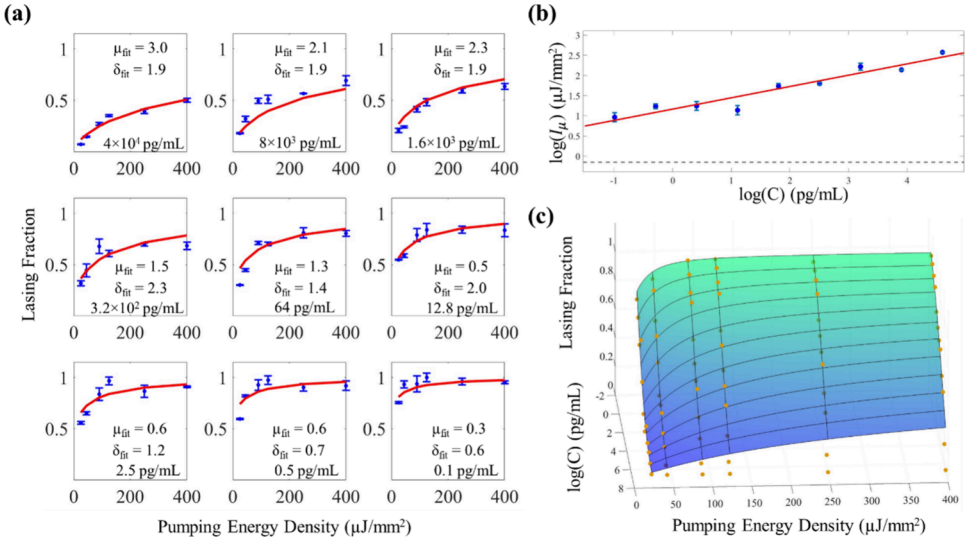

Figure 5. (a) Calibration curves obtained using function fitting of the lasing fraction vs the pumping energy density for the nine sets of data in Figure 4. Each subfigure represents the lasing fraction of an ME with respect to the pumping energy density for a given analyte concentration in solution (C). The function fitting is performed using eq 2. μ_{fit} and σ_{fit} refer to the fitted values for the Gaussian distribution. For all nine sets of data, I_{norm} and I_0 are calculated to be 17.74 and 0.71 μJ/mm^2, respectively. E is set to 1 for the fitting. Note that in the above function fitting, the three sets of data from the three highest concentrations (5×10^6, $1 \times 10,^6$ and 2×10^5 pg/mL) are not included, since their lasing fractions are close to zero, which do not provide enough information for the Gaussian distribution. (b) Calibration lines for I_μ vs the analyte concentration in the log−log scale. The gray dashed line is the reference line for $\log(I_0)$, which corresponds to the logarithmic of the lasing threshold of microlasers in the absence of analyte. (c) 3D fitted surface plot of the lasing fraction of the microlaser ensemble with respect to the pumping energy density and the analyte (streptavidin) concentration. The surface fitting is shown with scattered experimental data (dots). Error bars are omitted for the surface plot for clarity. Here, $\log(C)$ refers to the logarithmic analyte concentration in units of pg/mL. Note that some data points appear darker than others, meaning that they are below the surface, whereas others are on or above the surface.

Supporting Information Section S2. From here on, we will use the normalized lasing fraction data.

From Figure 4b, we can see that when those microlasers are incubated with analytes of various concentrations, the (normalized) lasing fraction curves that originally converge at 0 pg/mL start to diverge. For example, at 0.1 pg/mL, the lasing fraction is about 75% for the pumping energy density of 25 μJ/mm^2, whereas the lasing fraction remains nearly 100% for the pumping energy density of 400 μJ/mm^2, which indicates that the number of quenchers (hence the number of analytes) varies from one microlaser to another, which results in a lasing threshold distribution among the microlasers. When different pumping energy densities are used for a given analyte concentration, we probe the analyte distribution on the ME, which has previously been discussed in the Working Principle section. Note that in a hypothetical scenario in which the number of quenchers (or the number of analytes) is the same for all microlasers, the lasing fraction curves should collapse to a single curve (i.e., all curves are completely overlapped).

The lasing fraction curves in Figure 4b can be treated as a group of calibration curves analogous to the calibration curve used in the conventional ELISA. The differences are that in our method, we have multiple calibration curves (six in Figure 4b), whereas in the conventional ELISA, only one calibration curve is available. Note that in conventional fluorescence based immunoassays, multiple calibration curves can be generated via

https://doi.org/10.1021/acssensors.5c00251
ACS Sens. 2025, 10, 6436−6445

different pumping power as well. However, due to the linear nature of the fluorescence intensity with respect to the pumping power, all calibration curves provide the same information and can be reduced to a single calibration curve after linear rescaling (see the illustration in Figure S2). In contrast, due to the nonlinear nature of the laser that has threshold behavior, the calibration curves in Figure 4b are linearly independent and fundamentally determined by the analyte distribution on the microlasers. These multiple calibration curves work together to help pinpoint the analyte concentration and enable a larger dynamic range than a single curve in the conventional ELISA.

Analyte Concentration Recovery Using the MQE. The MQE presented in eq 1 and the Gaussian distribution of the quenchers (analytes) on microlasers establish the connection between the lasing fraction and three variables: the pumping energy density and the two Gaussian parameters (the mean value μ and the standard deviation σ) of the distribution of the analytes on the ME, which is reflected in eq 2. Furthermore, the average number of analytes in the ME, μ, is positively related to the analyte concentration in solution (C), which is similar to digital ELISA where the average number of bright microunits is related to the analyte concentration in solution. Since μ is an intermediate parameter, eventually, the relationship among the lasing fraction, the pumping energy density, and the analyte concentration C, which parameters are all experimentally measurable, can be established by calibration curves obtained experimentally using function fitting of the lasing fraction of the ME with respect to the experimental pumping energy density using eq 2.

In the fitting process, the three constants in eq 2, E, I_0, and I_{norm}, are held constant for each set of ME data, since these constants are related to the experimental conditions such as enzyme/substrate type and microlaser properties, which are the same for all sets of MEs. For each set of ME incubated in one analyte concentration C_h, two Gaussian parameters, μ_h and σ_h can be used to describe its lasing fraction distribution. In the data fitting process, the Gaussian parameter pair for all sets of ME used in fitting (μ_h and σ_h, where h runs from 1 to M—the number of total sets of the MEs used in data fitting) and the three aforementioned constants (E, I_0, and I_{norm}) are fitted together to minimize the overall loss for all sets of the MEs. This fitting process guarantees that each data set shares the same parameters that describe the system, namely, E, I_0, and I_{norm}.

In our work, the function fitting (the lasing fraction vs the pumping energy density) is performed for the nine sets of data (i.e., $M = 9$) in Figure 4b with the analyte concentration ranging from 4×10^4 to 1×10^{-1} pg/mL, as shown in the subfigures of Figure 5a along with the corresponding fitted values of μ and σ (i.e., μ_{fit} and σ_{fit}). During the above function fitting, we drop three sets of data associated with excessively high analyte concentrations (5×10^6, 1×10^6, and 2×10^5 pg/mL), since their corresponding lasering fractions are low at all pumping energy densities and provide too few data points for a reliable Gaussian fit. For example, only one microlaser is bright in the 5×10^6 pg/mL set of ME. Note that μ_{fit} is not necessarily the actual average number of quenchers (or analytes) of the ME, since it is subject to a rescaling factor, i.e., the fitting constant E. This is because E is an unbounded parameter and contains information on quencher/enzyme (analyte) ratio during the incubation step. The exact value of E is determined by a microscopic quencher producing equation and it is unknown to us. However, from eq 2 we can see that while E is unbounded, the product, μE, is always fixed. Therefore, depending on the value of E that we choose, μ_{fit} varies and is rescaled by E. In our current work, E is set to be one ($E = 1$).

Figure 5b plots the calibration curve for I_μ vs the analyte concentration, showing good linearity in the logarithmic scale. We can use the above calibration curve to obtain the analyte concentration for a sample under test. We will first measure the lasing fraction of an ME at different pumping energy densities. Then the lasing fraction vs the pumping energy density will be fitted to the Gaussian cumulative distribution function, eq 2, where the parameter, μ, can be calculated (the values of E, I_0, and I_{norm} will remain the same as those used during calibration curve generation). Then the calculated μ will be transformed to an I_μ value using eq 4. Finally, the analyte concentration can be recovered by checking the calculated I_μ value with the calibration curve in Figure 5b. I_μ is obtained through the fitting of an ME over multiple pumping energy densities (six in our current work) for significantly improved stability and robustness of measurements over single-point measurement (such as fluorescence measurement).

In Figure 5b, we plot the reference line for $\log(I_0)$ as the gray dashed line. I_0 is the fitted value for the lasing threshold in the absence of analytes, as indicated by eq 4. Based on these values, we can calculate the detection limit for our system. From experiment measurements, the $\log(I_\mu)$ value for 0.1 pg/mL group is 0.96, and the $\log(I_\mu - 2\sigma_{exp})$ value of this point is 0.55. Therefore, I_μ is more than $2\sigma_{exp}$ larger than $\log(I_0)$ (with a value of -0.15). Since $\log(I_0)$ is the recovered lasing threshold value for the negative control, our detection limit is at least 0.1 pg/mL.

Based on the linearity of I_μ and the analyte concentration in the logarithmic scale, we then performed 3D fitting of the lasing fraction vs the analyte concentration vs the pumping energy density. The fitted surface is presented in Figure 5c, showing the continuous change of the lasing fraction with respect to the analyte concentration and the pumping energy density. Figure 5b,c show that our system is continuously responsive over a concentration change of more than 5 orders of magnitude and achieves a low detection limit of 0.1 pg/mL.

Note that this 3D surface also works as a calibration surface (in 3D) that functions like a calibration curve in conventional ELISA (2D). The 3D calibration surface allows for pinpointing the concentration of the analyte under test using only one pumping energy density. In this case, the sample under test will incubate with an ME, then the lasing fraction will be measured at only one pumping energy density. A point on the calibration surface will be located with the measured lasing fraction under the given pumping energy density, which provides the value of the analyte concentration. Although a single-point measurement is faster and simpler than the function-fitting method that we demonstrated here, it lacks stability and may lead to large measurement errors.

Our assay platform was also tested for IL-6 measurements using the assay protocol mentioned in the Materials and Methods section. The results can be found in the Supporting Information Section S5.

DISCUSSION

In this work, we proposed and demonstrated a new bioassay platform that uses microlaser ensembles to probe the distribution of analytes among the microlasers and sub-

https://doi.org/10.1021/acssensors.5c00251
ACS Sens. 2025, 10, 6436−6445

sequently deduce the analyte concentration in solution using a statistical model. Our method is fundamentally different from digital ELISA.

The limitation in digital detection is that while it can distinguish one analyte from zero analytes for each microunit, it is unable to differentiate one from two or more analytes in each microunit. As illustrated in Figure S3a, the presence of two or more analytes in a microunit saturates the system. Therefore, digital ELISA relies on a fundamental assumption that the average number of analytes per microunit is far below one. When the average number of analytes per microunit approaches one for the entire ensemble, significant deviations arise. Consequently, digital ELISA has a limited dynamic range (especially in the upper range of detection).

In contrast, our microlasers, as microunits, have tunable dynamic ranges, which can be achieved by tuning the external pumping. This concept is mathematically described in eq 2 and schematically illustrated in Figure S3b, which allows our system to achieve a large dynamic range. The current assumption in our method is that the number of analytes exceeds the number of microunits (microlasers in our current work), so that we can use the Gaussian distribution. In the future, when even lower analyte concentrations are pursued, a new statistical model can be developed that may provide an even more sensitive detection and larger dynamic range.

Furthermore, both digital ELISA and conventional ELISA provide only one calibration curve. In digital ELISA, it is the average number of analytes vs the analyte concentration. In conventional ELISA, it is the detection signal (such as light intensity or absorption) vs the analyte concentration. In contrast, due to the threshold behavior intrinsic to lasers, our method has multiple calibration curves.

Essentially, our method is to map the analyte distribution among detection microunits (microlasers in our case). This is similar to digital ELISA, which also maps the distribution of the analytes in an ensemble of microunits but at a very low average number of analytes per microunits. Alternatively, we can use the conventional fluorescence-based method to detect the light intensity from individual detection microunit to map the distribution, which, unlike digital ELISA, does not require the average number of analytes per microunit be far below one. However, according to our theoretical analysis,[47] our microlaser quenching method has a sensitivity orders of magnitude greater than that of a fluorescence-based method. Therefore, our method is more accurate in obtaining the analyte distribution information.

While a single microlaser has previously been used as a biosensor to recover the analyte concentration through laser intensity measurement[50] or laser onset time measurement,[51] these single-point measurements do not provide stable and robust data, as discussed previously. Moreover, the laser onset time method[51] requires extremely long assay time and the long time exposure to the external pumping light may bleach the gain medium, leading to reduced sensitivity and a large variation.

CONCLUSIONS

In this work, we presented the theory and experimental realization of the microlaser ensemble quenching bioassay platform that is fundamentally different from digital ELISA. Using streptavidin and biotin binding assay as a model system, we demonstrated that this system is sensitive, achieving a detection limit of 0.1 pg/mL and can have a dynamic range of exceeding 5 orders of magnitude. Our system uses the assumption of Gaussian distribution for analyte numbers and thus can effectively recover high analyte concentrations. Our platform has an advantage in diagnostic applications where test-sample biomarkers can span multiple orders of magnitude.

In the future, we will extend the dynamic range in both the low and high end of analyte concentrations. To detect lower concentrations of analytes, quenchers with a higher quenching strength can be used. This approach will make the microlaser more sensitive to the quenching effect caused by a lower number of analytes (or quenchers) associated with the microlaser. More homogeneous microlasers can also be explored to reduce the lasing fraction variances in measurements, thus helping the system to reach lower concentrations. To detect higher concentrations of analytes, larger pumping energy densities (>400 $\mu J/mm^2$) can be used to pump the ME, so that we can observe more bright microlasers to perform function fitting. We will also validate our method using complex samples such as serum and saliva, to study if the matrix effect from the complex media would affect the performance of the system, particularly at the lower analyte concentration end. Another research direction that can be pursued is spectral-multiplexed detection that takes advantage of narrow lasing emission spectral line width, which allows the detection of different lasing wavelengths from different dyes within even a single-color channel (e.g., green color).[52] Finally, with the recent development in integrated photonics fabrications, some other types of microlasers with high homogeneity and low cost can be explored. Ring resonator arrays, which do not rely on external F−P cavities, and VCSELs, which are made of semiconductor materials with high uniformity (i.e., microlaser homogeneity) and are pumped electrically, can be used to implement this platform.

ASSOCIATED CONTENT

Supporting Information

The Supporting Information is available free of charge at https://pubs.acs.org/doi/10.1021/acssensors.5c00251.

Description of the image data processing method to count the microlasers, equation for counting the microlasers, comparison between the microlaser quenching method and the fluorescence-based method, and early results for IL-6 measurements (PDF)

AUTHOR INFORMATION

Corresponding Author

Xudong Fan − *Department of Biomedical Engineering, Center for Wireless Integrated MicroSensing and Systems (WIMS²), and Max Harry Weil Institute for Critical Care Research and Innovation, University of Michigan, Ann Arbor, Michigan 48109, United States;* orcid.org/0000-0003-0149-1326; Email: xsfan@umich.edu

Authors

Weishu Wu − *Department of Biomedical Engineering, Center for Wireless Integrated MicroSensing and Systems (WIMS²), and Max Harry Weil Institute for Critical Care Research and Innovation, University of Michigan, Ann Arbor, Michigan 48109, United States;* orcid.org/0000-0002-2325-3946

Yuhang Cao − *Department of Biomedical Engineering, Center for Wireless Integrated MicroSensing and Systems (WIMS²), and Max Harry Weil Institute for Critical Care Research and*

https://doi.org/10.1021/acssensors.5c00251
ACS Sens. 2025, 10, 6436−6445

Innovation, University of Michigan, Ann Arbor, Michigan 48109, United States

Xiaotian Tan − *Shenzhen Institute of Advanced Technology, Chinese Academy of Science, Shenzhen, Guangdong 518071, P. R. China;* orcid.org/0000-0001-5529-8092

Complete contact information is available at: https://pubs.acs.org/10.1021/acssensors.5c00251

Notes

The authors declare the following competing financial interest(s): X.F. is an inventor of the laser emission technologies used in this work, which are licensed to LEMX Health Technology Co., LTD. He and the University of Michigan have financial interests in LEMX.

■ ACKNOWLEDGMENTS

The authors thank the support from Richard A. Auhll Professorship from the University of Michigan.

■ REFERENCES

(1) Wild, D. *The Immunoassay Handbook: Theory and Applications of Ligand Binding, ELISA and Related Techniques*; Newnes, 2013.
(2) Hage, D. S. Immunoassays. *Anal. Chem.* **1999**, *71*, 294−304.
(3) Surugiu, I.; Danielsson, B.; Ye, L.; Mosbach, K.; Haupt, K. Chemiluminescence imaging ELISA using an imprinted polymer as the recognition element instead of an antibody. *Anal. Chem.* **2001**, *73*, 487−491.
(4) Herrmann, M.; Veres, T.; Tabrizian, M. Enzymatically-generated fluorescent detection in micro-channels with internal magnetic mixing for the development of parallel microfluidic ELISA. *Lab Chip* **2006**, *6*, 555−560.
(5) Pei, K.; Xiong, Y.; Xu, B.; Wu, K.; Li, X.; Jiang, H.; Xiong, Y. Colorimetric ELISA for ochratoxin A detection based on the urease-induced metallization of gold nanoflowers. *Sens. Actuators, B* **2018**, *262*, 102−109.
(6) Chen, S.; Svedendahl, M.; Van Duyne, R. P.; Käll, M. Plasmon-enhanced colorimetric ELISA with single molecule sensitivity. *Nano Lett.* **2011**, *11*, 1826−1830.
(7) Hempen, C.; Karst, U. Labeling strategies for bioassays. *Anal. Bioanal. Chem.* **2006**, *384*, 572−583.
(8) O'Donnell, C. M.; Suffin, S. C. Fluorescence immunoassays. *Anal. Chem.* **1979**, *51*, 33A−40A.
(9) Goldman, E. R.; Medintz, I. L.; Mattoussi, H. Luminescent quantum dots in immunoassays. *Anal. Bioanal. Chem.* **2006**, *384*, 560−563.
(10) Thürer, R.; Vigassy, T.; Hirayama, M.; Wang, J.; Bakker, E.; Pretsch, E. Potentiometric immunoassay with quantum dot labels. *Anal. Chem.* **2007**, *79*, 5107−5110.
(11) Lv, Y.; Wang, F.; Li, N.; Wu, R.; Li, J.; Shen, H.; Li, L. S.; Guo, F. "Development of dual quantum dots-based fluorescence-linked immunosorbent assay for simultaneous detection on inflammation biomarkers," Sens. *Actuators, B* **2019**, *301*, No. 127118.
(12) Seydack, M. Nanoparticle labels in immunosensing using optical detection methods. *Biosens. Bioelectron.* **2005**, *20*, 2454−2469.
(13) Kongsuwan, N.; Xiong, X.; Bai, P.; You, J.-B.; Png, C. E.; Wu, L.; Hess, O. Quantum plasmonic immunoassay sensing. *Nano Lett.* **2019**, *19*, 5853−5861.
(14) Ling, J.; Li, Y. F.; Huang, C. Z. Visual sandwich immunoassay system on the basis of plasmon resonance scattering signals of silver nanoparticles. *Anal. Chem.* **2009**, *81*, 1707−1714.
(15) Helle, M.; Boeije, L.; de Groot, E.; de Vos, A.; Aarden, L. Sensitive ELISA for interleukin-6: detection of IL-6 in biological fluids: synovial fluids and sera. *J. Immunol. Methods* **1991**, *138*, 47−56.
(16) Gratacos, J.; Collado, A.; Filella, X.; Sanmarti, R.; Canete, J.; Llena, J.; Molina, R.; Ballesta, A.; Muñoz-Gómez, J. Serum cytokines (IL-6, TNF-α, IL-1β and IFN-γ) in ankylosing spondylitis: a close correlation between serum IL-6 and disease activity and severity. *Rheumatology* **1994**, *33*, 927−931.
(17) Khan, S. A.; Joyce, J.; Tsuda, T. Quantification of active and total transforming growth factor-β levels in serum and solid organ tissues by bioassay. *BMC Res. Notes* **2012**, *5*, 636.
(18) Jayasena, S.; Smits, M.; Fiechter, D.; De Jong, A.; Nordlee, J.; Baumert, J.; Taylor, S. L.; Pieters, R. H.; Koppelman, S. J. Comparison of six commercial ELISA kits for their specificity and sensitivity in detecting different major peanut allergens. *J. Agric. Food Chem.* **2015**, *63*, 1849−1855.
(19) Al-Hosary, A. A. T.; Ahmed, J.; Nordengrahn, A.; Merza, M. Assessment of the first commercial ELISA kit for the diagnosis of theileria annulata. *J. Parasitol. Res.* **2015**, *2015*, No. 787812.
(20) Rissin, D. M.; Kan, C. W.; Campbell, T. G.; Howes, S. C.; Fournier, D. R.; Song, L.; Piech, T.; Patel, P. P.; Chang, L.; Rivnak, A. J.; Ferrell, E. P.; Randall, J. D.; Provuncher, G. K.; Walt, D. R.; Duffy, D. C. Single-molecule enzyme-linked immunosorbent assay detects serum proteins at subfemtomolar concentrations. *Nat. Biotechnol.* **2010**, *28*, 595−599.
(21) Hwang, J.; Banerjee, M.; Venable, A. S.; Walden, Z.; Jolly, J.; Zimmerman, C.; Adkisson, E.; Xiao, Q. Quantitation of low abundant soluble biomarkers using high sensitivity single molecule counting technology. *Methods* **2019**, *158*, 69−76.
(22) Byrnes, S. A.; Huynh, T.; Chang, T. C.; Anderson, C. E.; McDermott, J. J.; Oncina, C. I.; Weigl, B. H.; Nichols, K. P. Wash-free, digital immunoassay in polydisperse droplets. *Anal. Chem.* **2020**, *92*, 3535−3543.
(23) Cohen, L.; Cui, N.; Cai, Y.; Garden, P. M.; Li, X.; Weitz, D. A.; Walt, D. R. Single molecule protein detection with attomolar sensitivity using droplet digital enzyme-linked immunosorbent assay. *ACS Nano* **2020**, *14*, 9491−9501.
(24) Song, Y.; Ye, Y.; Su, S.-H.; Stephens, A.; Cai, T.; Chung, M.-T.; Han, M. K.; Newstead, M. W.; Yessayan, L.; Frame, D.; Humes, H. D.; Singer, B. H.; Kurabayashi, K. A digital protein microarray for COVID-19 cytokine storm monitoring. *Lab Chip* **2021**, *21*, 331−343.
(25) Gao, Z.; Song, Y.; Hsiao, T. Y.; He, J.; Wang, C.; Shen, J.; MacLachlan, A.; Dai, S.; Singer, B. H.; Kurabayashi, K.; Chen, P. Machine-learning-assisted microfluidic nanoplasmonic digital immunoassay for cytokine storm profiling in COVID-19 patients. *ACS Nano* **2021**, *15*, 18023−18036.
(26) Wu, C.; Dougan, T. J.; Walt, D. R. High-throughput, high-multiplex digital protein detection with attomolar sensitivity. *ACS Nano* **2022**, *16*, 1025−1035.
(27) Chen, C.; Porter, R.; Zhou, X.; Snozek, C. L.; Yang, E. H.; Wang, S. Microfluidic digital immunoassay for point-of-care detection of NTproBNP from whole blood. *Anal. Chem.* **2024**, *96*, 10569−10576.
(28) https://www.quanterix.com/.
(29) https://www.quanterix.com/product-brochures/ss-simoa-il-17a-advantage-plus/.
(30) https://www.quanterix.com/product-brochures/ss-measure-ultra-low-levels-of-ifn-%CE%B1-with-simoa-advantage-plus/.
(31) Belushkin, A.; Yesilkoy, F.; Altug, H. Nanoparticle-enhanced plasmonic biosensor for digital biomarker detection in a microarray. *ACS Nano* **2018**, *12*, 4453−4461.
(32) Zhang, W.; Dang, T.; Li, Y.; Liang, J.; Xu, H.; Liu, G. L.; Hu, W. "Digital plasmonic immunosorbent assay for dynamic imaging detection of protein binding," Sens. *Actuators, B* **2021**, *348*, No. 130711.
(33) Yang, S.-M.; Bi, Q.; Zhang, W. J.; Cui, X.; Zhou, Y.; Yuan, C.; Cui, Y. Highly accurate multiprotein detection on a digital ELISA platform. *Lab Chip* **2022**, *22*, 3015−3024.
(34) Rissin, D. M.; Kan, C. W.; Song, L.; Rivnak, A. J.; Fishburn, M. W.; Shao, Q.; Piech, T.; Ferrell, E. P.; Meyer, R. E.; Campbell, T. G.; Fournier, D. R.; Duffy, D. C. Multiplexed Single Molecule Immunoassays. *Lab Chip* **2013**, *13*, 2902−2911.
(35) Liu, X.; Sun, Y.; Lin, X.; Pan, X.; Wu, Z.; Gai, H. Digital duplex homogeneous immunoassay by counting immunocomplex labeled with quantum dots. *Anal. Chem.* **2021**, *93*, 3089−3095.

(36) Zhang, Q.; Li, J.; Pan, X.; Liu, X.; Gai, H. Low-numerical aperture microscope objective boosted by liquid-immersed dielectric microspheres for quantum dot-based digital immunoassays. *Anal. Chem.* **2021**, *93*, 12848−12853.
(37) Zhang, Y.; Noji, H. Digital bioassays: theory, applications, and perspectives. *Anal. Chem.* **2017**, *89*, 92−101.
(38) Zhang, J.; Wiener, A. D.; Meyer, R. E.; Kan, C. W.; Rissin, D. M.; Kolluru, B.; George, C.; Tobos, C. I.; Shan, D.; Duffy, D. C. Improving the accuracy, robustness, and dynamic range of digital bead assays. *Anal. Chem.* **2023**, *95*, 8613−8620.
(39) Chen, Q.; Liu, H.; Lee, W.; Sun, Y.; Zhu, D.; Pei, H.; Fan, C.; Fan, X. Self-assembled DNA tetrahedral optofluidic lasers with precise and tunable gain control. *Lab Chip* **2013**, *13*, 3351−3354.
(40) Martino, N.; Kwok, S. J. J.; Liapis, A. C.; Kim, H.-M.; Wu, S. J.; Wu, J.; Forward, S.; Jang, H.; Dannenberg, P. H.; Jang, S.-J.; Lee, Y.-H.; Yun, S.-H. Wavelength-encoded laser particles for massively multiplexed cell tagging. *Nat. Photonics* **2019**, *13*, 720−727.
(41) Wu, X.; Chen, Q.; Xu, P.; Chen, Y.-C.; Wu, B.; Coleman, R. M.; Tong, L.; Fan, X. Nanowire lasers as intracellular probes. *Nanoscale* **2018**, *10*, 9729−9735.
(42) Wu, X.; Wang, Y.; Chen, Q.; Chen, Y.-C.; Li, X.; Tong, L.; Fan, X. High-Q, low-mode-volume microsphere-integrated Fabry-Pérot cavity for optofluidic lasing applications. *Photon. Res.* **2019**, *7*, 50−60.
(43) Aas, M.; Chen, Q.; Jonáš, A.; Kiraz, A.; Fan, X. Optofluidic FRET lasers and their applications in novel photonic devices and biochemical sensing. *IEEE J. Sel. Top. Quantum Electron.* **2016**, *22*, 188−202.
(44) Lacey, S.; White, I. M.; Sun, Y.; Shopova, S. I.; Cupps, J. M.; Zhang, P.; Fan, X. Versatile opto-fluidic ring resonator lasers with ultra-low threshold. *Opt. Express* **2007**, *15*, 15523−15530.
(45) Moon, H.-J.; Chough, Y.-T.; An, K. Cylindrical microcavity laser based on the evanescent-wave-coupled gain. *Phys. Rev. Lett.* **2000**, *85*, 3161.
(46) Siegman, A. E. *Lasers*; University Science Books, 1986.
(47) Wu, W.; Cao, Y.; Tan, X.; Fan, X. Sensitive bioassay with an ultra-large dynamic range via microlaser ensemble quenching. *arXiv preprint arXiv:2501.15299*, 2025.
(48) Chen, Q.; Chen, Y.-C.; Zhang, Z.; Wu, B.; Coleman, R.; Fan, X. An integrated microwell array platform for cell lasing analysis. *Lab Chip* **2017**, *17*, 2814−2820.
(49) Wu, W.; Zhang, Y.; Tan, X.; Chen, Y.; Cao, Y.; Sahai, V.; Peterson, N.; Goo, L.; Fry, S.; Kathawate, V. Antigen-independent single-cell circulating tumor cell detection using deep-learning-assisted biolasers. *Biosens. Bioelectron.* **2025**, *271*, No. 116984.
(50) Gong, C.; Gong, Y.; Khaing Oo, M. K.; Wu, Y.; Rao, Y.; Tan, X.; Fan, X. Sensitive sulfide ion detection by optofluidic catalytic laser using horseradish peroxidase (HRP) enzyme. *Biosens. Bioelectron.* **2017**, *96*, 351−357.
(51) Wu, X.; Oo, M. K. K.; Reddy, K.; Chen, Q.; Sun, Y.; Fan, X. Optofluidic laser for dual-mode sensitive biomolecular detection with a large dynamic range. *Nat. Commun.* **2014**, *5*, 3779.
(52) Chen, Y.-C.; Tan, X.; Sun, Q.; Chen, Q.; Wang, W.; Fan, X. Laser-emission imaging of nuclear biomarkers for high-contrast cancer screening and immunodiagnosis. *Nat. Biomed. Eng.* **2017**, *1*, 724−735.

https://doi.org/10.1021/acssensors.5c00251
ACS Sens. 2025, 10, 6436−6445